ELSEVIER

Journal of Photochemistry and Photobiology A: Chemistry 110 (1997) 131–139

Journal of PHOTOCHEMISTRY AND PHOTOBIOLOGY A: CHEMISTRY

Photophysics and intramolecular excimer formation in a constrained anthracenyl diadduct

Z. Lin, S. Priyadarshy, A. Bartko, D.H. Waldeck *

Department of Chemistry, University of Pittsburgh, Pittsburgh, PA 15260, USA

Received 3 March 1997; revised 27 May 1997; accepted 2 June 1997

Abstract

The photophysical properties of *N,N'*-di(9-anthracylmethyl)hexahydropyrimidine **1** and its analogues are reported. The electronic spectra and kinetics of these compounds are studied over a range of solvent and temperature conditions. It is shown that the unique structure of **1** leads to the formation of a very stable ($\tau = 120$ ns) anthracenyl diadduct. The results also suggest that the viscosity, but not the polarity, of the solvent plays an important role in excimer formation. © 1997 Elsevier Science S.A.

Keywords: Anthracenyl diadduct; *N,N'*-Di(9-anthracylmethyl)hexahydropyrimidine; Intramolecular excimer formation; Photophysics

1. Introduction

A number of workers have studied the photophysics and photochemistry of bichromophoric molecules. In the majority of these systems, the chromophores are connected via tethers which allow a large number of conformations. This study explores the photophysics of a new bichromophoric system, the anthracene diadduct *N,N'*-di(9-anthracylmethyl)-hexahydropyrimidine **1** (Scheme 1), in which the number of available conformations is constrained. In addition, the important influence of the solvent on the reaction dynamics is investigated. Excimer formation in **1** appears to be strongly influenced by the distance and strain between the chromophores.

Compound **1** can undergo two reactive relaxation processes in the excited state: excimer formation and electron transfer (or exciplex formation). It does not appear to form the well-known anthracene photodimer, presumably because of the steric constraints designed into the molecule between the two anthracene chromophores. In this work, we examine the available relaxation pathways and their solvent dependence. In addition, the reaction coordinate for excimer formation occurs within well-defined geometrical constraints compared with other less constrained systems [1–4]. The presence of the nitrogen atoms in the central ring introduces an electron transfer channel, i.e. transfer from the nitrogen lone pair to the anthracene acceptor. This quenching of the local emission of anthracene has also been reported for other amine systems [5–7]. The two reaction channels, excimer formation and electron transfer quenching, are competitive processes. The solvent viscosity and dielectric properties (polarity) modify these reaction rates, but in different ways. For example, the viscosity plays an important role in excimer

Molecular Structures

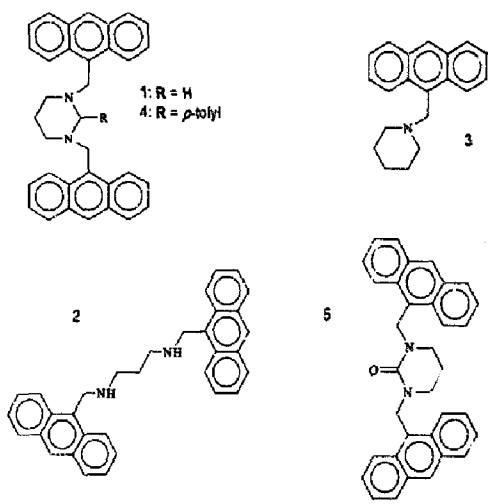

Scheme 1.

* Corresponding author.

PII S1010-6030(97)00193-7

formation, but is not so important in electron transfer. Conversely, a change in polarity has little effect on excimer formation.

Before describing the present results, it is useful to review previous work. The excimer properties of anthracene and its derivatives are quite rich. However, the excimer emission of anthracene in solution was not reported until 1976 [8]. The anthracene excimer exhibits weak emission because of the efficient formation of the photodimer of anthracene [2]. It has been postulated [3,9] that the excimer of anthracene is a precursor to the formation of the photodimer. A number of workers [10,11] have studied intramolecular excimer formation in anthracene diadducts. When the anthracenes are constrained from forming the photodimer, excimer emission is observed. Other researchers have shown that substitution at the 9 and 10 positions of anthracene allows intermolecular excimer formation, but prohibits photodimer formation. To summarize, the excimer will proceed to form the photodimer efficiently unless the system is geometrically constrained.

A very detailed and fruitful study of the anthracene excimer was performed by Hayashi et al. [10]. By synthesizing a series of anthracenophanes and dianthrylethanes, these workers were able to show that the anthracene excimer can exist over a range of geometries (see Fig. 1). In addition, they showed that the distinct excimer geometries have different stabilities and that only a subset of the excimers proceeds onwards to form the photodimer. On a qualitative level, we may deduce a "rule of thumb" from their work. For geometries in which the anthracene rings overlap by a single phenyl unit (type I), the excimer emission has a peak in the 460 nm region. For geometries in which the anthracenes overlap by two phenyl units (type II), the excimer is more stable than type I and the emission is in the 570 nm region. For geometries in which the anthracenes overlap by three phenyl units (type III), the excimer is most stable and emission occurs in the 620 nm region. Although oversimplified, this rule of thumb shows that the position of the excimer emission reflects the extent of physical overlap of the anthracene ring systems.

This work is structured into four sections. In Section 2, the details of the synthetic, computational and physical methods are described. In Section 3, the spectral observations, solvent effects on the excimer kinetics, structural characterization of the compounds and theoretical calculations are described. In Section 4, these observations are used to produce a model for the photophysical and photochemical relaxation pathways. Finally, some conclusions are drawn.

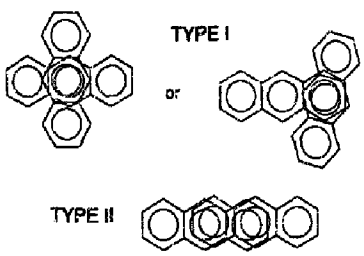

Fig. 1. Two types of anthracene excimer: type I, one phenyl ring overlapped; type II, two phenyl rings overlapped. These geometries correlate with distinct spectral emissions.

2. Experimental details

2.1. Solvents

All solvents were purchased from Aldrich unless otherwise specified. The hydrocarbons, other than methylcyclohexane, were used as received. Methylcyclohexane was distilled over sodium. Other solvents were purified according to standard procedures [12].

2.2. Synthesis

The synthesis of **1** is described here. In 50 ml of anhydrous ethanol, 4.12 g (20 mmol) of 9-anthraldehyde was mixed with 0.74 g (10 mmol) of 1,3-propyldiamine. The mixture was heated to reflux for 1 h and then cooled to room temperature. The imine precipitated from solution and was collected by filtration (4.2 g was collected (93%)). The product was used directly for the next reaction step. The imine (2.25 g, 5 mmol) was placed in 80 ml of isopropanol with 2 g of $NaBH_4$ under a positive pressure of nitrogen. The solution was refluxed for 20 h. After cooling to room temperature, the solution was further cooled in an ice–water bath. At this point, crystallites formed and were filtered (1.9 g was collected (85%)). This compound is **2** (Scheme 1; verified by ^1H nuclear magnetic resonance (NMR) and melting point 109–110 °C). Using a 50 ml Erlenmeyer flask, the above product (0.23 g, 0.5 mmol) was dissolved in 20 ml of anhydrous ethanol, to which a few drops of formaldehyde (37% in H_2O) were added. The solution was heated by a steam bath for 10 min. After standing and cooling, needle-like crystals formed (0.2 g, 87%). This product was repeatedly recrystallized. The melting point of the final product **1** was 192–192.5 °C. The identity of **1** was verified by ^1H NMR and high resolution mass spectrometry.

Compound **4** was prepared by adding *p*-methylbenzaldehyde instead of formaldehyde in the procedure outlined for **1**. Compound **4** was purified by recrystallization and its identity was verified by high resolution mass spectrometry. The melting point of **4** was 211–213 °C. Compound **5** (*N,N'*-di(9-anthracylmethyl)tetrahydropyrimid-2-one) was prepared by adding diphenyl carbonate instead of formaldehyde in the procedure outlined for **1**. Single crystals of **5** were obtained from a solvent mixture of methylene chloride–ether. The crystallographic analysis was performed by Steve Geib of the University of Pittsburgh, using a Siemens P3 diffractometer (Mo Kα) (see Fig. 7).

The compound *N*-(9-anthracylmethyl)piperidine **3** (melting point, 130–131 °C) was synthesized by adapting a literature procedure [13]. Its identity was verified by ^1H NMR and high resolution mass spectrometry.

2.3. Instrumentation

A range of commercial instrumentation was employed in these studies. An SLM 8000 fluorometer was used for the fluorescence and excitation spectra and an IBM UV–visible (model 9420) absorption spectrometer was used for the absorption measurements. Both NMR spectroscopy (Bruker 300 MHz) and mass spectrometry (V.G. Fisons 70-G) were used to identify and characterize the compounds prepared.

The time-resolved fluorescence transients were measured using the time-correlated, single-photon counting technique. A general introduction to this technique is available [14] and specific features of this apparatus have been described previously [15]. Some items have changed since this report. In particular, a DB10 dispersion-free monochromator was used in the detection arm and the fluorescence photons were detected with a microchannel plate photomultiplier tube (containing 6 μm channels. Hamamatsu R3809U). The decay transients were fitted to a sum of exponentials by iterative convolution with a measured instrument response function and the Marquardt–Levenburg algorithm was used to optimize the goodness of fit. Typical χ^2 values ranged from 1.0 to 1.5.

3. Results

3.1. Steady state spectroscopy

Fig. 2 shows the fluorescence spectra of species **1**, **2**, **3**, **4** and 9-methylanthracene in methylcyclohexane. These spectra were obtained at room temperature and at a sample optical density (OD) of 0.1 for an excitation wavelength of 366 nm. The spectra in Fig. 2 are normalized to the emission intensity at 411 nm. The reference spectrum in Fig. 2 is that of 9-methylanthracene, which clearly reveals vibronic structure in the local emission band and no broad emission. Fig. 2(a) shows that compounds **1**, **2** and **3** have a vibronically resolved emission band, similar to 9-methylanthracene, and, in addition, a contribution from a broad structureless emission at the red edge. The spectra of **2** and **3** show a slight distortion from the reference spectrum, but only **1** has a dramatic broad emission band. Fig. 2(b) compares the emission spectrum of **1** with that of compound **4** which contains a tolyl moiety on the pyrimidine ring between the anthracenes. Compound **4** shows the vibronic structure observed in **1–3**, but does not exhibit a strong, structureless emission at the red edge. The emission spectrum of compound **5** is not plotted in Fig. 2, because it is indistinguishable from that of 9-methylanthracene. From a consideration of these data and the molecular structures, it can be concluded that the enhanced broad emission in **1** is related to the spatial overlap of the anthracene moieties: excimer formation. In addition, it is clear that the weaker broad emission is not related to this interaction between the anthracene rings.

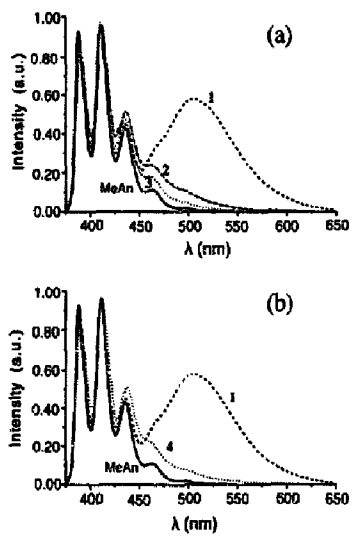

Fig. 2. Emission spectra of 9-methylanthracene and compounds **1**, **2** and **3** are shown in (a). Spectra for 9-methylanthracene and **1** and **4** are shown in (b). The broad structureless emission, indicative of the excimer, is apparent for compound **1**. A weak, red-shifted emission is also evident for compounds **2–4**. 9-Methylanthracene (———); **1** (– – –); **2** (– · –); **3** (· · ·).

The spectra were also studied as a function of the concentration of the chromophore. For species **1**, the relative magnitude of the broad emission does not change with concentration (from 10^{-5} to 10^{-4} M), in contrast with the monomer (or local) emission. Except for an overall intensity change and the minor effects of self-absorption on the blue edge, the spectra are identical. A concentration dependence of the emission spectrum of **3** (from 10^{-5} to 10^{-4} M) gives a similar result. These results show that the broad emission band in these species results from intramolecular rather than intermolecular processes.

The absorption and excitation spectra of the compounds were also studied. The absorption spectra of compounds **1–5** are fairly similar. This observation suggests that the electronic interaction between the anthracene rings in the ground state is small. In addition, the excitation spectrum of **1** was studied at three different emission wavelengths (388 nm in the monomer band, 505 nm in the broad emission band and 550 nm in the broad emission band). The excitation spectra are identical, indicating that the initially excited state is the same for the different emission bands.

The overall intensity of the luminescence emission depends on the solvent polarity, but the spectral position of the emission is not a strong function of the solvent polarity. Table 1 shows the relative quantum yields of emission for compound **1**. It is clear from these data that the total emission quantum yield decreases significantly as the solvent polarity increases. Fig. 3 shows the emission difference spectra for **1** in four solvents (methylcyclohexane, methanol, acetonitrile and CH_2Cl_2). The 9-methylanthracene spectrum, which does not change noticeably between these solvents, was used as reference. The difference spectra were computed by subtract-

Table 1
Quantum yield[a] data for **1** in different solvents at room temperature

Solvent	ϕ_{total}	ϕ_{EX}/ϕ_{total}	ϵ	η (cP)
Methylcyclohexane	0.11	0.49	0.024	0.679
CH_2Cl_2	0.0095	0.57	8.93	0.413
Methanol	0.0083	0.42	33.0	0.54
Acetonitrile	0.0013	0.42	36.64	0.369
Polystyrene	–	0.0	–	–

[a]All quantum yields are referenced to 9-methylanthracene (0.33) [16]. ϵ is the static dielectric constant; η is the solvent shear viscosity; ϕ_{total} is the total emission quantum yield; ϕ_{EX} is the excimer quantum yield.

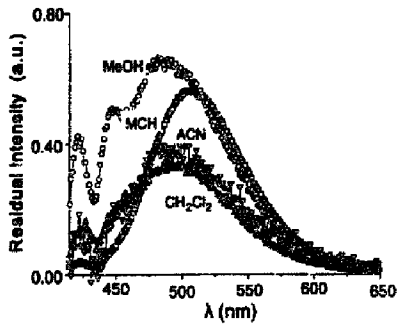

Fig. 3. Emission difference spectra for **1** in methylene chloride (CH_2Cl_2), methylcyclohexane (MCH), acetonitrile (ACN) and methanol (MeOH).

Table 2
Quantum yield data in different solvents at room temperature

Solvent	1	2	3	4
Methylcyclohexane	0.11	–	0.028	0.32
CH_2Cl_2	0.0095	0.13	0.0045	0.33
Methanol	0.0083	0.014	0.0045	0.30
Acetonitrile	0.0013	0.0075	<0.0010	0.29

ing the emission spectrum of 9-methylanthracene from the emission spectrum of **1** (all spectra were normalized at 411 nm before subtraction). The broad emission does not shift strongly with solvent polarity; however, the range of polarities available for study was restricted because of strong quenching. In addition, the relative quantum yield of the excimer (ϕ_{EX}/ϕ_{total}) does not change significantly between solvents. These observations indicate that the broad, red-shifted emission of **1** does not have significant charge transfer character. For compounds **1–4**, the overall emission quantum yield is strongly quenched by more polar solvents (Table 2).

3.2. Spectroscopy and kinetics of excimer emission in 1

3.2.1. Temperature dependence

The relative intensities of the local and excimer emission in the steady state emission spectrum of **1** in methylcyclohexane vary as a function of the temperature. Fig. 4(a) shows the emission spectrum as a function of the temperature. It is clear that the monomer emission decreases with increasing temperature and that the broad (or excimer) emission increases with increasing temperature (note the clear presence of an isoemissive point). Fig. 4(b) shows a plot of the relative quantum yield of the local and excimer emission as a function of the temperature. This plot demonstrates that the total fluorescence yield is relatively flat over this temperature range, whereas the relative amounts of excimer and local emission change. It is clear from these curves that the formation of the excimer decreases as the temperature of the solvent decreases, and this trend is reflected in an opposite dependence for the monomer emission. With the caveat that the temperature range is only 40 °C (from −14 °C to 24 °C), an activation energy of 5 kJ mol^{-1} is found.

3.2.2. Viscosity dependence

Solvent studies reveal that the excimer emission is influenced by the solvent viscosity [17]. Fig. 5(a) shows the emission spectra for **1** in several hydrocarbon solvents. A good correlation is found between the quantum yields of excimer emission and the viscosities of straight chain alkane solvents (Fig. 5(b)). Further evidence for the viscosity dependence comes from the spectra of **1** in a frozen matrix (methylcyclohexane at 77 K) and in the solid phase (polystyrene at 298 K). For both of these conditions, no evidence of the broad emission band is found. When methylcyclohexane is melted and the polystyrene is dissolved in methylene chloride, the broad band reappears. These results demonstrate the sensitivity of the broad band emission to the solvent viscosity.

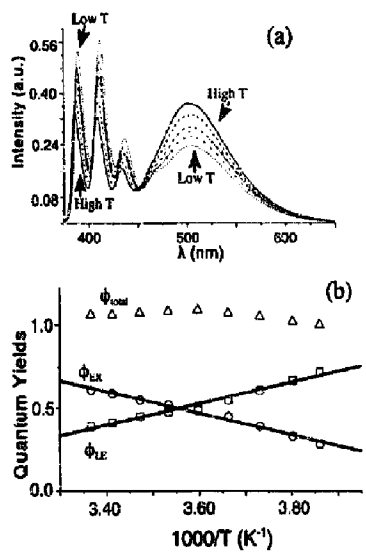

Fig. 4. (A) Emission spectra recorded at different temperatures for **1** in methylcyclohexane. (B) Temperature dependence of the quantum yields for the excimer (ϕ_{EX}), monomer (ϕ_{LE}) and total emission (ϕ_{total}) (see text for details).

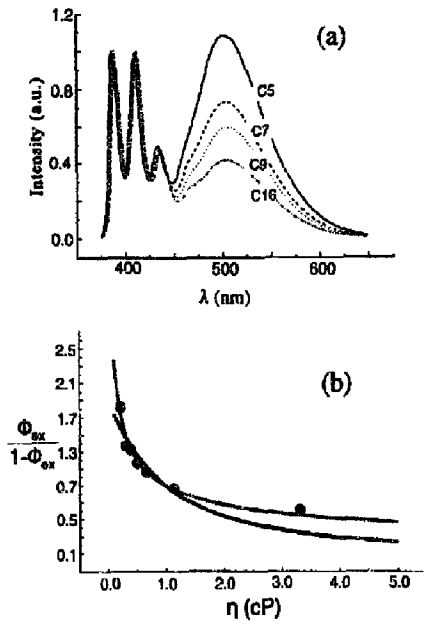

Fig. 5. (A) Emission spectra of **1** in alkane solvents at 298 K. Each spectrum is labelled by the number of carbon atoms in the solvent. (B) Ratio of excimer to monomer quantum yield for the spectra as a function of the solvent viscosity. The broken line shows a fit to a power law form (Eq. (1)) and the full line shows a fit to the hydrodynamic Kramers model (Eq. (2)).

3.2.3. *Time-resolved spectroscopy*

The time-resolved fluorescence decay of **1** was measured at different emission wavelengths in methylcyclohexane at room temperature. The results are presented in Table 3. Because of the red tail of the monomer emission and, possibly, the weak exciplex emission, it is somewhat difficult to determine accurately the risetime of the excimer emission. Three excimer emission decays, taken at different wavelengths, are plotted in Fig. 6. The risetime of the decay curve increases as the observation wavelength(s) is moved to the red. This shift occurs because the excimer emission becomes less contaminated by the monomer emission as the wavelength is moved to the red. A comparison of the decay parameters for the monomer and excimer kinetics shows the expected behaviour, i.e. the risetime of the excimer approaches the decay time of the monomer. This contamination of the excimer emission by the monomer has been reported previously in related systems [11,18].

3.3. *Structural studies of compounds 1 and 5*

Two sets of structural investigations were performed: crystal structures and computational studies.

It was possible to prepare single crystals of **5** and obtain crystal structures. For comparison, a geometry of **5** was computed by performing a geometry optimization at the AM1 level [19]. The crystal structure and computed geometry are

Table 3
Decay parameters for the monomer and excimer emissions of **1** in methylcyclohexane at different emission wavelengths

λ (nm)	τ_1 (%)	τ_2 (%)	τ_3 (%)
410	–	0.84 (98.9)	5.9 (1.1)
540	0.16 (−100)	0.76 (50)	112.0 (50)
570	0.09 (−100)	–	116.0 (100)
600	0.08 (−74)	0.63 (−26)	120.6 (100)
630	0.10 (−74)	0.65 (−26)	118.7 (100)

The decay profiles were fitted to a sum of up to three exponentials. The lifetimes τ are reported in nanoseconds.

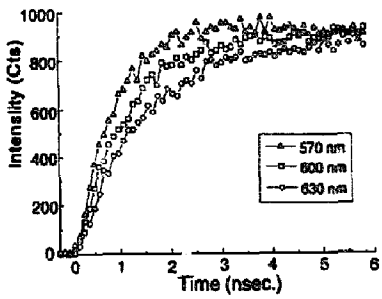

Fig. 6. Early time behaviour of the emission profile of **1** in methylcyclohexane at three different emission wavelengths.

plotted together in Fig. 7. In this figure, the crystal structure of **5** is represented by full lines and the computed structure is represented by broken lines. The solvent molecules (methylene chloride) shown here were in the actual crystal structure, but were not present in the computational structure. The average difference in position is 0.18 Å atom^{-1}. The good agreement between the crystal geometry and the computed geometry demonstrates that this level of theory is useful as a qualitative and semiquantitative guide for the probable molecular geometries.

Molecular geometries were computed for compounds **1** and **3–5** at the semiempirical level of quantum theory. A full geometry optimization was performed for all molecules using the AM1 hamiltonian. A normal mode analysis was performed at the same level of theory to confirm that the ground state geometry thus obtained was not a transition state. The optimized geometries for **1**, **4** and **5** are shown in Fig. 8. The upper figure in each panel shows the entire molecule, whereas the lower figure has the bridging unit removed so that the relative orientation of the anthracene rings is more apparent. Table 4 contains some of the relevant geometrical parameters for these structures. The anthracenes in **1** are nearly planar with an angle between the two ring planes of about 20°. The shortest distance between the rings is 4.4 Å. In fact, approximately two of the aromatic rings of the two covalently linked anthracenes overlap with each other. By contrast, the diamide functionality in **5** changes the ring geometry so that the anthracenes are further apart, making excimer formation less likely. The optimized geometry of **4** leads to similar conclusions. The presence of the tolyl group causes a distortion of

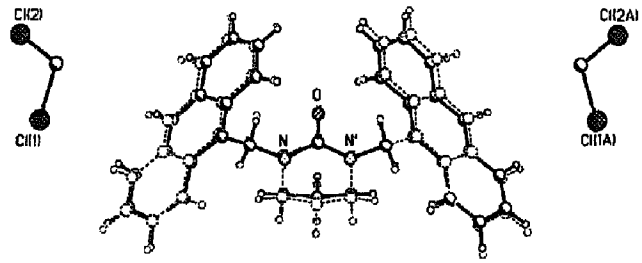

Fig. 7. Crystal structure obtained for **5** (full lines). Superimposed on this structure is a structure for **5** (broken lines) computed using AM1.

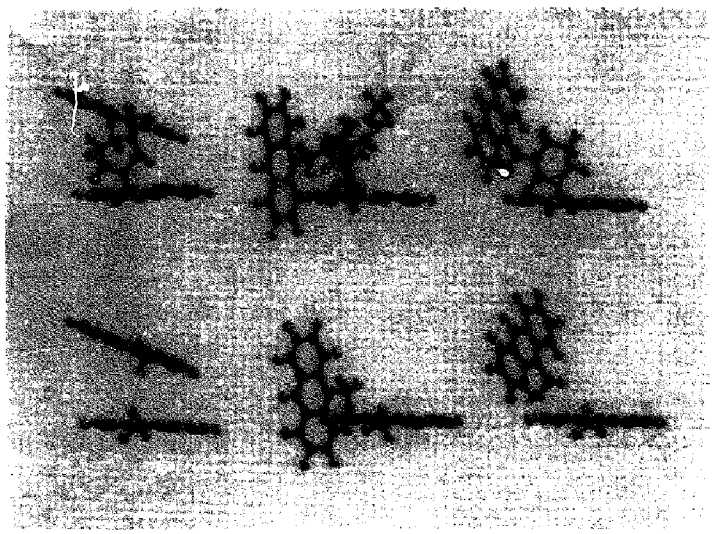

Fig. 8. Most stable geometries, found using AM1, for molecules **1**, **4** and **5**. The upper figure shows the entire molecule and the lower figure has the bridging unit removed.

Table 4
Summary of some of the geometrical parameters computed for the different anthracenyl diadducts

Molecule	Angle between long axes	Angle between 9–10 and 9'–10' axes	9–9' distance	Angle between N–C–C9 and N'–C'–C9'
1	23	5.2	4.92	120.2/121.0
3	–	–	–	120.1/–
4	12.0	109.0	5.42	115.4/114.4
5	30.0	129.5	6.77	115.8/115.8

the structure away from that of **1** so that the anthracene rings are rotated to a nearly perpendicular interplanar orientation. It is clear from these results that compound **1** has a favourable geometry for overlap of the anthracene ring planes.

3.4. *Theoretical calculations*

The optimized geometries were used to compute the self-consistent field (SCF) molecular orbitals and their energies at the AM1 [19] and INDO [20] levels. The spectroscopic properties were obtained using the version (INDO/S) suitable for the reproduction of experimental UV–visible spectra. The ground state calculation was followed by a configuration interaction of the 101 lowest single excited configurations from the INDO/S ground state. Transition moments were calculated using the dipole length operators. The calculated oscillator strengths within the INDO/S level are known to be overestimated [21].

The molecular orbitals and energies for all the molecules were obtained within the supermolecule model [22]. In this model, molecular orbitals are generated for the entire molecule. The advantages of performing supermolecule calculations are twofold. First, it is easier to perform the calculations and, second, it has been shown by Chandra and Lim [23] that these calculations can be used to explain the excimer properties. The energies of the frontier orbitals for molecules

Table 5
Computed state energies and oscillator strengths for compounds **1**, **4** and **5**

State	Energy of **1**	*f* of **1**	Energy of **4**	*f* of **4**	Energy of **5**	*f* of **5**
S_1	29259	0.030	29329	0.210	29409	0.260
S_2	29539	0.005	29538	0.030	29593	0.015
S_3	29573	0.041	29595	0.030	29597	0.067
S_4	29990	0.452	29888	0.320	29880	0.350

The energies are given in units of cm^{-1} and *f* is the oscillator strength.

1, **4** and **5** are shown in Table 5. Also shown are the contributions from the two anthracene rings to the wavefunctions. An analysis of the few highest occupied molecular orbitals (HOMOs) of molecule **1** reveals that HOMO, HOMO − 1 and HOMO − 2 are delocalized over the two anthracene moieties. An analysis of the few lowest unoccupied molecular orbitals (LUMOs) reveals that LUMO, LUMO + 1 and LUMO + 2 are localized on either anthracene for molecule **1**. In fact, the HOMO has contributions of 60% and 40% from "ring 1" and "ring 2" respectively, while HOMO − 1 has 40% and 60% contributions from "ring 1" and "ring 2". HOMO − 2 has equal contributions from the two anthracenes. Energetically, HOMO and HOMO − 1 are nearly degenerate with a splitting of around 0.019 eV, whilst LUMO and LUMO + 1 are also nearly degenerate with a splitting of 0.014 eV.

This delocalization should be contrasted with the results for the related molecule **4**. For **4**, the frontier orbitals are more localized than in the case of **1**. For **4**, HOMO, HOMO − 3, LUMO + 1 and LUMO + 3 are localized on "ring 1" and HOMO − 1, HOMO − 4, LUMO and LUMO + 2 are localized on "ring 2". HOMO − 2 is localized on the phenyl ring between the two anthracene rings. The splitting of HOMO and HOMO − 1 is 0.051 eV, whilst that of LUMO and LUMO + 1 is 0.155 eV. Similar conclusions may be drawn for the orbital structure of molecule **5**. In the case of **5**, the splitting of HOMO and HOMO − 1 is 0.047, and that of LUMO and LUMO + 1 is 0.029.

Molecule **3** provides a useful reference point because it contains only one anthracene ring. The HOMO and LUMO of **3** are shifted to lower energy with respect to those of 9-methylanthracene. The two singlet excited states of **3** are calculated to be S_1 at 28 536 cm^{-1} and S_2 at 29 065 cm^{-1}, with oscillator strengths of 0.019 and 0.250 respectively. The relative size of these oscillator strengths agrees well with expectations for the excitation of the L_a and L_b states of anthracenes. The four excited states of **1**, **4** and **5** result from the two close-lying excited states (in **3** they are only separated by 0.1 eV) on each anthracene ring and the interaction of these states between the two rings. For **1**, the calculations indicate that the first three excited states have a small value for the oscillator strength from the HOMO, while the S_1 states of **4** and **5** have much larger oscillator strengths. An analysis of the excited states of these molecules reveals that the localized excited state in each ring contributes approximately 48% to the S_1 state of **4**, thus leaving a contribution of 4% coming from transitions between the rings. The nature of S_4 is similar to that of S_1. The S_2 and S_3 states have nearly 50% contributions for each of the "inter" ring transitions. A similar analysis holds for molecule **5**. In molecule **1**, the transitions from the ground state to excited states S_1, S_2 and S_3 have larger or equal contributions from excitations between the anthracene rings compared with excitations within the anthracene rings. In contrast, the transition to S_4 of **1** has almost 100% contribution from within the anthracene ring. It seems reasonable that the excitation studied in the experiments above involves an initial excitation into S_4, with a subsequent emission from S_4 for the local emission and from one or more of the other singlet states for the excimer emission. In the cases of **4** and **5**, the two rings are nearly perpendicular (see Table 4) and hence the mixing of the orbitals is different from that of **1**. A detailed analysis of the wavefunctions and mixing of the various configurations will be presented elsewhere.

The calculated absorption spectra for these compounds show similar trends to those observed in the experiments. All the compounds show strong absorption near the same wavelength. This supports the conclusion that the interaction between the rings in the ground state is small. The presence of the strong excimer fluorescence for **1** is supported by the fact that the rings are more or less parallel to each other, but are not totally superposed. The distance between the two rings is more than 4.0 Å.

4. Discussion

The spectra presented in Figs. 2–5 support the assignment of the broad emission in **1** to the anthracene excimer. In particular, the spectra in Fig. 2(A) demonstrate that two anthracene moieties and the pyrimidine ring system must be present in order to generate a strong broad emission. In addition, the data in Fig. 2(B) show that the placement of steric bulk between the two anthracene moieties eliminates the broad emission observed in **1**. The observation that no excimer emission is found for **5** demonstrates that the pyrimidine ring geometry plays a significant role in determining the excimer yield. The spectral studies in polar solvents demonstrate that the weak broad emission observed for the other compounds (**2**–**4**) probably arises from a process involving significant charge rearrangement, possibly an exciplex. The observation that the relative quantum yield of excimer formation (ϕ_{EX}/ϕ_{total}) is independent of the solvent polarity

further supports the assignment of the broad emission in **1** to the excimer. The spectra in Figs. 4 and 5 show that the yield of the excimer is strongly dependent on the temperature and viscosity in non-polar solvents. Finally, the kinetic data presented in Table 3 and Fig. 7 support the excimer model for species **1**. The combination of these data provides a compelling argument for the assignment of the strong broad emission to the anthracene excimer.

With the exception of its strong intensity, the broad emission band for **1** is consistent with previous work on the anthracene excimer. This emission band has a maximum very similar to that reported by Hayashi et al. [10] for what they term the type II excimer. The two excimer types differ in both their geometry (degree of overlap) and stability (see Fig. 1). The position of the excimer emission reported for **1** is in agreement with the spectrum of [2.2](1,4)(9,10)anthracenophane [10], in which two of the aromatic rings of the anthracene moieties overlap. This interpretation is further supported by the quantum chemical calculations of the geometry of **1**. Interestingly, the excimer emission reported here is observed at room temperature, in contrast with Ref. [10], where type II emission was only observed at 77 K (much weaker emission at room temperature). Hence it appears that the excimer formed by the two anthracene moieties in **1** is quite stable, but constrained from forming the photodimer.

Excimer formation is influenced by the viscosity and temperature of the solvent. These observations are consistent with the need for the two anthracene moieties to undergo a large amplitude motion in finding the excimer geometry. In part, the temperature dependence is probably caused by this viscosity effect, but may also reflect an intrinsic barrier to the reaction. Disentangling these two contributions to the temperature dependence is left for a future study. The viscosity-dependent data at a single temperature were compared with two simple models for the excimer formation rate (see Fig. 6(B)). The broken curve in this figure represents a best fit of the data to a power law form for the formation rate of the excimer, i.e.

$$\frac{\phi_{EX}}{1-\phi_{EX}} = \frac{B}{\eta^a} \quad (1)$$

The curve in Fig. 6(B) has best-fit parameters of $B = 0.895$ cP and $a = 0.420$. The full curve in this figure represents a best fit of the data to the Kramers form for the rate, i.e.

$$\frac{\phi_{EX}}{1-\phi_{EX}} = G\eta\left(\sqrt{1+(F/\eta)^2}-1\right) \quad (2)$$

where G and F are parameters. The best-fit parameters are $F = 1.23$ cP and $G = 1.52$ cP^{-1}. These models are commonly used to treat rate processes of this type [24,25]. The comparisons shown in Fig. 6(B) demonstrate that the observations are largely in agreement with the trends predicted by the models. A more rigorous analysis will require a more detailed study of the temperature and pressure dependence of the excimer formation rate in non-polar solvents.

The data for compounds **1–4** also reveal a strong dependence of the total emission quantum yield (see Table 1) on the solvent polarity. This dependence is assigned to an additional relaxation channel involving charge rearrangement in the molecule, probably via electron transfer (or exciplex formation) between the lone pair on the nitrogen and the anthracene ring. A literature precedent [5,6] exists for this process. The weak broad emission in compounds **2–4** may reflect radiative recombination involving charge transfer. This emission is weak and is strongly quenched as the solvent polarity is increased. It is probable that this emission is present in **1** also, but is not observed because of the strong excimer emission. In contrast with the excimer emission in **1**, the weak emission in **3** does not show a significant viscosity or temperature dependence. Further support for this assignment arises from **5** whose spectrum is insensitive to the solvent polarity. The nitrogen atoms in this compound are in an amide bonding environment, rather than the amine environment in compounds **1–4**.

5. Conclusions

This work provides an examination of the photophysical and photochemical relaxation pathways in the anthracenyl diadduct **1**. This model system displays competition between two relaxation pathways. In non-polar solvents, the system displays a significant yield of excimer. The excimer formation yield is dependent on the viscosity, temperature and polarity of the medium. The kinetics of excimer formation can reasonably be explained by a simple kinetic scheme involving one conformer; however, spectral overlap of the monomer and excimer emission bands prohibits this conclusion from being shown unequivocally. In polar solvents, the yield of excimer is greatly reduced. This reduction is assigned to electron transfer quenching of the initially excited state, rather than to any change in the intrinsic excimer formation rate. The photophysical system reported here shows an interesting competition between the two relaxation pathways, which can be controlled by the solvent. A more comprehensive and thorough understanding of this system may provide an interesting avenue for a better comprehension of the solvent's role in relaxation phenomena and chemical reaction dynamics.

Acknowledgements

We acknowledge financial support of this work by the PRF (Grant 25179-AC6,4) and partial support by the National Science Foundation (Grant CHE-9416913).

References

[1] J. Birks, Photophysics of Aromatic Molecules, Wiley, New York, 1970. N. Turro, Modern Organic Photochemistry, Benjamin-Cummings, Menlo Park, CA, 1978. J. Vandendriessche, R.

Goedeweeck, P. Collart, F.C. De Schryver, Photophysical and Photochemical Tools in Polymer Science, Reidel, New York, 1986, p. 226.
[2] T.A. Smith, D.A. Shipp, G.D. Scholes, K.P. Ghiggino, J. Photochem. Photobiol. A: Chem. 80 (1994) 177. F.C. De Schryver, P. Collart, J. Vandendriessche, R. Goedeweeck, A.M. Swinnen, M. Van der Auweraer, Acc. Chem. Res. 20 (1987) 160. K.A. Zachariasse, W. Kuhnle, U. Leinhos, P. Reynders, G. Striker, J. Phys. Chem. 95 (1991) 5476. E.M. Buchberger, B. Mollay, W.-D. Weixelbaumer, H.F. Kauffmann, W. Klopffer, J. Chem. Phys. 89 (1988) 635. R. Andriessen, F.C. De Schryver, N. Boens, N. Ikeda, H. Masuhara, Macromolecules 22 (1989) 2166.
[3] A. Castellan, J.-P. Desvergne, H. Bouas-Laurent, Chem. Phys. Lett. 76 (1980) 390.
[4] A. Castellan, J.-P. Desvergne, J.R. Lesclaux, J.-C. Soulignac, Chem. Phys. Lett. 106 (1984) 117. J.-P. Desvergne, N. Bitit, A. Castellan, M. Webb, H. Bouas-Laurent, J. Chem. Soc., Perkin Trans. II (1988) 1885. H. Yao, T. Okada, N. Mataga, J. Phys. Chem. 93 (1989) 7388.
[5] M.R. Wasielewski, D.W. Minsek, M.P. Niemczyk, W.A. Svec, N.C. Yang, J. Am. Chem. Soc. 112 (1990) 2823.
[6] M.E. Huston, K.W. Haider, A.W. Czarnik, J. Am. Chem. Soc. 110 (1988) 4460. J.C. Beeson, M.E. Huston, D.A. Pollard, T.K. Venkatachalam, A.W. Czarnik, J. Fluor. 3 (1993) 65.
[7] A.M. Brouwer, R.D. Mout, P.H. Maasen van den Brink, H.J. van Ramesdonk, S.A. Jonker, Chem. Phys. Lett. 180 (1991) 556. N.C. Yang, J. Libman, J. Am. Chem. Soc. 95 (1973) 5783. N. Mataga, T. Kubota, Molecular Interactions and Electronic Spectra, Marcel Dekker, New York, 1970. H. Beens, H. Knibbe, A. Weller, J. Chem. Phys. 47 (1967) 1183.
[8] J.F. McVey, D.M. Shold, N.C. Yang, J. Chem. Phys. 65 (1976) 3375.
[9] M.D. Cohen, A. Ludmer, V. Yakhot, Chem. Phys. Lett. 38 (1976) 398. E.A. Chandross, J. Chem. Phys. 38 (1965) 4175. E.A. Chandross, J. Ferguson, E.G. McRae, J. Chem. Phys. 45 (1965) 3546.
[10] T. Hayashi, N. Mataga, Y. Sakata, S. Misumi, M. Morita, J. Tanaka, J. Am. Chem. Soc. 98 (1976) 5910.
[11] M.A. Fox, P.F. Britt, J. Phys. Chem. 94 (1990) 6351. J. Ferguson, A. Castellan, J.-P. Desvergne, H. Bouas-Laurent, Chem. Phys. Lett. 78 (1980) 446.
[12] D.D. Perrin, W.L.F. Armarego, Purification of Laboratory Chemicals, 3rd ed., Pergamon, New York, 1988.
[13] R.A.W. Johnston, M.E. Rose, Tetrahedron 35 (1979) 2169.
[14] D.V. O'Connor, D. Phillips, Time-Correlated Single Photon Counting, Academic Press, New York, 1984.
[15] D.M. Zeglinski, D.H. Waldeck, J. Phys. Chem. 92 (1988) 692.
[16] C.A. Parker, T.A. Joyce, Chem. Commun. (1967) 744.
[17] K. Hara, S. Akimoto, H. Suzuki, Chem. Phys. Lett. 175 (1990) 493. Y.B. Chung, D.-J. Jang, D. Kim, M. Lee, H.S. Kim, B.H. Boo, Chem. Phys. Lett. 176 (1991) 453. K.A. Zachariasse, G. Duveneck, R. Busse, J. Am. Chem. Soc. 106 (1984) 1045.
[18] M. Itoh, K. Fuke, S. Kobayashi, J. Chem. Phys. 72 (1980) 1417.
[19] M.J.S. Dewar, E.G. Zoebisch, E.F. Henly, J.J.P. Stewart, J. Am. Chem. Soc. 107 (1985) 3902.
[20] J.A. Pople, D.L. Beveridge, P.A. Dobosh, J. Chem. Phys. 47 (1967) 2026. J.A. Pople, D.L. Beveridge, Approximate Molecular Orbital Theory, Wiley, New York, 1974. J. Ridley, M. Zerner, Theor. Chim. Acta 32 (1973) 111.
[21] M.C. Zerner, Review of Computational Chemistry, Wiley, New York, 1996, p. 313.
[22] M.S. Gudipati, J. Phys. Chem. 98 (1994) 9750.
[23] A.K. Chandra, E.C. Lim, J. Chem. Phys. 49 (1968) 5066.
[24] D.H. Waldeck, Chem. Rev. 91 (1991) 415. J.T. Hynes, Theory of Chemical Reactions, vol. 4, CRC, New York, 1985.
[25] Y.-P. Sun, J. Saltiel, J. Phys. Chem. 93 (1989) 6246. J. Saltiel, S.A. Waller, D.F. Sears, Jr., E.A. Hoburg, D.M. Zeglinski, D.H. Waldeck, J. Phys. Chem. 98 (1994) 10 689.